Polymorphism, Fluorescence, and Optoelectronic Properties of a Borazine Derivative

Simon Kervyn,[a] Oliver Fenwick,[b] Francesco Di Stasio,[b] Yong Sig Shin,[b] Johan Wouters,[a] Gianluca Accorsi,*[c] Silvio Osella,[d] David Beljonne,*[d] Franco Cacialli,*[b] and Davide Bonifazi*[a, e]

Abstract: We have prepared a new borazine derivative that bears mesityl substituents at the boron centers and displays exceptional chemical stability. Detailed crystallographic and solid-state fluorescence characterizations revealed the existence of several polymorphs, each of which showed different emission profiles. In particular, a bathochromic shift is observed when going from the lower- to the higher-density crystal. Computational investigations of the conformational dynamics of borazine **1** in both the gas phase and in the solid state using molecular dynamics (MD) simulations showed that the conformation of the peripheral aryl groups significantly varies when going from an isolated molecule (in which the rings are able to flip over the 90° barrier at RT) to the crystals (in which the rotation is locked by packing effects), thus generating specific nonsymmetric intermolecular interactions in the different polymorphs. To investigate the optoelectronic properties of these materials by fabrication and characterization of light-emitting diodes (LEDs) and light-emitting electrochemical cells (LECs), borazine **1** was incorporated as the active material in the emissive layer. The current and radiance versus voltage characteristics, as well as the electroluminescence spectra reported here for the first time are encouraging prospects for the engineering of future borazine-based devices.

Keywords: boron · doping · molecular modeling · nitrogen · polymorphism

Introduction

The abundance and availability of carbon as a natural element together with its ability to form different types of homoatomic covalent bonds allows the development of numerous types of fascinating bulky or discrete (nano)structures, each of which display unique structural, chemical, and physical properties.[1] Among others, polycyclic aromatic hydrocarbons (PAHs) possess many attractive electronic properties in terms of conductivity, adsorption, and emission properties.[1b, 2] Among the different functionalization strategies with hydrophobic, hydrophilic, electron-donating, or electron-withdrawing groups to tune their self-assembly, solubility, absorption, and emission behavior, the replacement of the carbon atoms with electron-deficient or/and electron-rich heteroatoms—that is, atom doping—in the all-carbon networks strongly affects the frontier orbitals, thus dramatically altering their electronic properties.[3] In particular, the replacement of two carbon atoms by one boron and one nitrogen atom in aromatic structures leads to isoelectronic structural mimics[3a,b,4] that possess local dipole moments as the bonding now contains a significant polarity contribution.[3b–d,4b] Such polarity is known to considerably alter the character of the frontier molecular orbitals, thus affecting the optical properties of the molecular system, and generally giving rise to larger energy gaps[5] than those of their all-carbon analogues. In this respect, the inorganic mimic of benzene, borazine, first reported by Stock et al. in 1926,[6] possesses a wide energy gap of approximately 6 eV,[7] although it displays similarities in both geometry and in formal topology of the π-molecular orbitals.[8] The UV-emissive properties of borazine and of its potential oligomeric derivatives[5,9] make such molecular substrates attractive candidates to be implemented as the active layer in UV-

[a] Dr. S. Kervyn, Prof. J. Wouters, Prof. D. Bonifazi
Department of Chemistry and Namur Research College (NARC)
University of Namur (UNamur), Rue de Bruxelles 61
Namur, 5000 (Belgium)
E-mail: davide.bonifazi@fundp.ac.be

[b] Dr. O. Fenwick, Dr. F. Di Stasio, Y. S. Shin, Prof. F. Cacialli
Department of Physics and Astronomy (CMMP Group) and
London Centre for Nanotechnology
University College London, Gower Street
London, WC1E 6BT (UK)
E-mail: f.cacialli@ucl.ac.uk

[c] Dr. G. Accorsi
Molecular Photoscience Group
Istituto per la Sintesi Organica e la Fotoreattività (ISOF)
Consiglio Nazionale delle Ricerche (CNR)
Via P. Gobetti 101, 40129 Bologna (Italy)
E-mail: gianluca.accorsi@isof.cnr.it

[d] Dr. S. Osella, Dr. D. Beljonne
Laboratory for Chemistry of Novel Materials
University of Mons; Place du Parc, 20, 7000 Mons (Belgium)
E-mail: david.beljonne@umons.ac.be

[e] Prof. D. Bonifazi
Department of Chemical and Pharmaceutical Sciences and
INSTM UdR Trieste, University of Trieste,
Trieste, Piazzale Europa 1, Trieste (Italy)

Supporting information for this article is available on the WWW under http://dx.doi.org/10.1002/chem.201204598.

light-emitting diodes (LEDs), and consequently for a number of potentially high-impact applications.[10] However, the susceptibility of the BN bonds to undergo hydrolysis in the presence of moisture (e.g., borazine rapidly decomposes to boric acid, ammonia, and H_2 in the presence of ambient humidity) has been a major deterrent to the widespread synthetic development of BN-doped aromatic hydrocarbons and their use in optoelectronic devices; to date, only one single example describing their role as charge transporter has been reported.[11] Attempts to significantly prevent the hydrolytic decomposition of borazines by introduction of various substituents were not successful until bulky substituents were placed in the *ortho* positions of *B*-aryl groups. In particular, following the works of Brown et al.[12] and Hawkins et al.[13] that described *B*-mesityl derivatives, in 1965 Nagasawa[14] reported an apparently moisture-stable *B*-triphenyl-*N*-trimesitylborazine that bore two methyl groups at the *ortho* positions of the aryl substituents. Recently, Yamaguchi and co-workers also reported stable borazine derivatives in which visible-emitting anthryl substituents were inserted at the B position.[15] Inspired by these approaches, in this work we have prepared a new borazine derivative that displays exceptional chemical stability, in which the B-atom centers bear mesityl substituents. Detailed crystallographic and fluorescence characterizations showed the existence of several polymorphs,[16] each of which showed a different emission profile in the solid state, thus suggesting a unique interplay between intermolecular forces and conformations. In particular, a redshifted emission emerges when passing from the lower- to the higher-density crystal. Molecular modeling simulations were performed to assess the electronic structure of the borazine derivatives and analyze their peculiar luminescence characteristics in the solid state. To investigate the emissive properties under an externally applied bias, light-emitting electrochemical cells (LECs) were fabricated by incorporating borazine **1** as the active material. These devices were then characterized by measurement of the current and radiance versus voltage characteristics, as well as of their electroluminescence spectra so as to enable the evaluation of the optoelectronic properties of the borazine-based active layer.

Results and Discussion

Synthesis and spectroscopic characterization: By following the facile synthetic procedure of Brown et al. and Groszos et al.,[17] trimesitylborazine derivative was synthesized by using a one-pot procedure that involved BCl_3, as shown in Scheme 1. The reaction of BCl_3 with aniline produced the corresponding *B*-trichloro-*N*-triphenylborazine, which was subsequently treated with the organometallic mesityl derivative (both Li-derived and Grignard reagents gave similar results) to afford *B*-trimesityl-*N*-triphenylborazine in a moderate yield (see the detailed experimental procedure and full characterization in the Supporting Information). The same procedure was also used for preparing reference hexaphe-
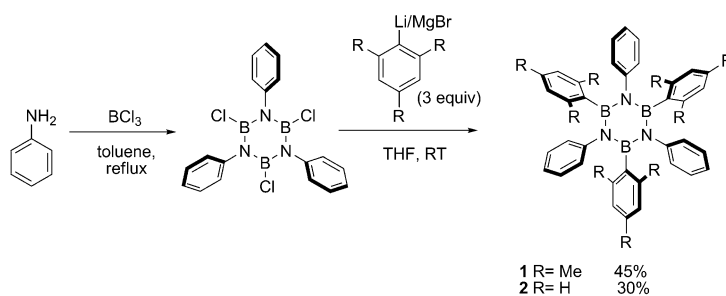
Scheme 1. Synthesis of borazines **1** and **2**.

nylborazine **2**. When subjected to hydrolysis in water-containing mixtures, compound **1** exhibited extraordinary stability, which suggested that the *ortho*-methyl substituents exert a steric hindrance, thus chemically shielding the B-atom centers. As expected, borazine **2** completely decomposes under the same conditions.

When compound **1** was crystallized from cyclohexane, CH_2Cl_2, or pentane, several polymorphs that belong to the $R\bar{3}c$, $R32$, and $P2_1/n$ space groups were obtained, respectively (for the crystallographic details, see the Supporting Information). In all polymorphs, the X-ray molecular structure reveals a deviation from orthogonal arrangement of the aryl substituents and the borazine ring with an interplanar angle between 63.14 to 83.68° depending on the polymorph and on the substituent (see below). As previously observed in other literature reports,[18] the intra-annular distance values between B and N atoms are between 1.40 and 1.46 Å, whereas the internal angle of the borazine cycle is between 114 and 124°. The central BN core is nearly planar with a torsion angle of approximately 1.5°. Similar structural characteristics have been also observed for molecule **2**.[18b]

The quasi-orthogonal arrangement of the aryl substituents forces the methyl substituents to nest atop the B atoms (C1−B1=3.0 Å), thus shielding the electrophilic atoms from nucleophilic addition reactions (Figure 1). Interestingly, mechanically grinding any of the formed crystals yielded the same crystalline powder (see XRD pattern in the Supporting Information) of an unknown space group, here labeled "powder X". As clearly seen from the crystal packing displayed in Figure 2, solid-state arrangements in the space groups $R32$ and $R\bar{3}c$ feature tubular voids with average diameters of 6.0 and 6.8 Å, respectively, whereas $P2_1/n$ crystals were revealed to be compact.

The electronic absorption spectra of borazine **1**, obtained in three different solvents (i.e., CH_2Cl_2, THF, and CH_3CN), cover the UV spectral window in the approximately 200–300 nm range, as depicted in Figure S17a in the Supporting Information. As expected, the excitation spectra fully match those of the corresponding absorption profiles, indicating the ligand-centered (LC) nature of the emitting states. The photoluminescence (PL) spectra in solution of the borazines along with those of molecular reference hexaphenylbenzene (HPB) are depicted in Figure 3. Remarkably, radiative emission is observed over spectral ranges that extend down to
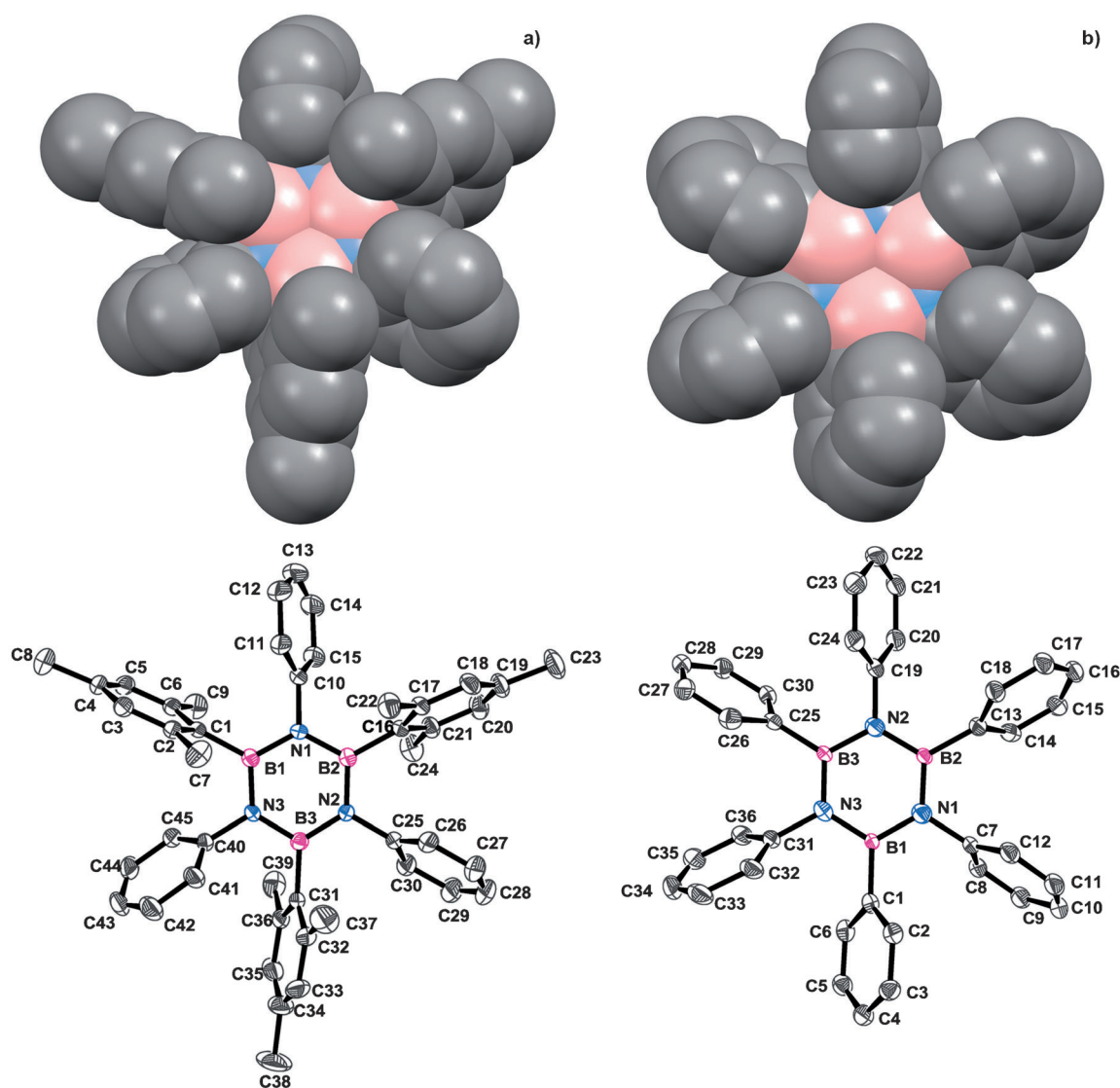
Figure 1. Space-filling (above) and ORTEP (below) representation of the X-ray crystal structure of borazines a) **1** (space group: $P2_1/n$) and b) **2** (space group: $Pna2_1$). B: pink, N: blue, C: gray. Hydrogen atoms are omitted for clarity.

less than 300 nm, which is in line with the expectation of significant UV-emitting species. No appreciable effect could be detected on the spectral profiles by changing the solvent polarity ($\varepsilon = 1.55$, 1.75, and 3.45 for CH_2Cl_2, THF, and CH_3CN, respectively; Figure S17b in the Supporting Information), as further confirmed by the photoluminescence quantum yields (Φ_{em}) and relative lifetimes (τ), which are substantially unchanged ($\Phi_{em} = 7.7\%$, $\tau = 7.1$ ns; $\Phi_{em} = 6.6\%$, $\tau = 7.2$ ns; and $\Phi_{em} = 7.2\%$, $\tau = 7.6$ ns in CH_2Cl_2, THF, and CH_3CN, respectively). In contrast, the solid-state emission features for the different borazine polymorphs of molecule **1** dramatically differ (Figure 3, bottom). To investigate the influence of the packing effects on the fluorescence properties, steady-state emission studies were performed. Depending on the different crystal packing, various emissive profiles that extended over a remarkably large spectral range (from <300 to >500 nm) were observed. Two main features are observed

around 310 and 360 nm, with relative intensities sensitive to the density of the solid: the PL of the more compact polymorph, $P2_1/n$, displays the most intense peak at approximately 360 nm, whereas the least compact polymorphs ($R32$ and $R\bar{3}c$) emit mostly at lower wavelength, very close to the solution case. In contrast, the total lifetimes (τ) are substantially similar ($\tau \approx 11$ ns) for all polymorphs, thus indicating similar deactivation processes.

Modeling of the electronic properties: To shed further light on the electronic structure and optical properties of the borazine derivatives both in solution and in the solid state, we resorted to ab initio time-dependent density functional theory (TD-DFT) and semiempirical (AM1/SCI[19] and INDO/SCI[20]) quantum-chemical calculations. Starting with the analysis of the one-electron energy diagram computed for borazines **1** and **2** and that of the reference HPB mole-
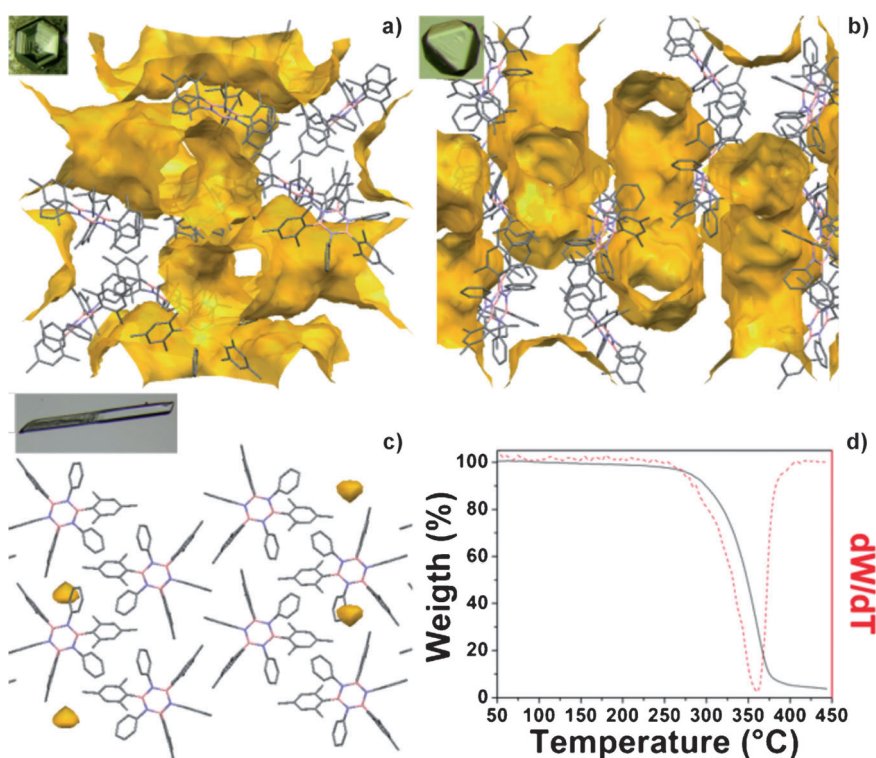
Figure 2. View of the crystal packing along the *c* axis of borazine **1** in space groups a) $R\bar{3}c$, b) $R32$, and c) $P2_1/n$. The yellow surfaces surround the crystal voids. d) TGA profile (black curve) and its derivative (red) of borazine **1** as obtained under an inert atmosphere.

(labeled iv in Table 1) that peaks at approximately 6 eV, the calculations also indicate a second less-intense band (labeled iii) together with a set of weakly optically allowed (labeled ii) and almost dark (labeled i) electronic transitions at lower energies.

For the sake of illustration, the INDO/SCI-simulated optical absorption spectrum of molecule **1** is displayed in Figure 5 together with the corresponding spectrum as measured in CH_3CN. A reasonable agreement is found between the experimental and theoretical results (although all predicted transitions are slightly redshifted relative to the experiment; Figure 5), with band iii appearing as a shoulder on the red side of the dominant band iv and a much weaker feature ii in the near-UV region. The lowest singlet electronic excitations computed at the INDO/SCI and AM1/SCI level are located

cule, the DFT/HSE[21] results displayed in Figure 4 (on the basis of geometric structures fully optimized at the HSE level using the polarized 6-31G* Gaussian basis set)[22] show a simultaneous (de)stabilization of the HOMO (LUMO) molecular orbital, which results in an increased energy bandgap upon going from HPB to hexaphenylborazine **2**. Notably, whereas the shape of the LUMO remains essentially unchanged, the HOMO shows smaller contributions on the central BN core in borazine **2** than that which derives from the central hexa-substituted phenyl ring of HPB (see Figure S21 in the Supporting Information). These changes reflect the partial ionic character of the BN bonds, as described by Molteni and co-workers.[10] As expected, the presence of weakly electron-donating methyl moieties on the mesityl groups in molecule **1** causes a minor high-energy shift of the frontier MOs relative to that of the naked hexaphenylborazine **2**.

To describe the nature of the lowest electronic excited states in borazine **1**, TD-DFT analysis using long-range corrected functionals (namely, CAM-B3LYP[23] and LC-ωPBE[24]) and semiempirical simulations were also performed. A consistent qualitative picture for the optical absorption spectrum of molecule **1** emerges from these calculations (although there are significant quantitative differences). These give rise to multiple electronic excitations that (based on their nature) can be collected in four bands, as depicted in Table 1. In addition to the very strong absorption

Table 1. Optical transitions calculated for a single molecule of borazine **1** at different levels of theory. The intensity of the transitions based on their relative oscillator strengths is indicated between the parentheses: very weak (vw), weak (w), medium (m), and strong (s).

Band label	CAM-B3LYP [eV]	LC-wPBE [eV]	INDO/SCI [eV]	AM1/SCI [eV]
i	5.1–5.3 (vw)	5.2–5.4 (vw)	4.29–4.38 (vw)	3.82–3.91 (vw)
ii	5.4–5.6 (m)	5.5–5.6 (w)	4.43–4.53 (w)	3.98–4.18 (w)
iii	5.7–5.8 (m)	5.9–6 (m)	5–5.5 (m)	5.3–5.5 (m)
iv	5.8–6.2 (s)	6–6.2 (s)	5.6–6.25 (s)	5.5–6.1 (s)

at around 4.3 and 3.8 eV, respectively, yet as these carry a vanishingly small oscillator strength they cannot be unambiguously identified on either the simulated or the measured spectrum. In a simplified picture, the spatial extent of the electronic excitations changes (the localization of the electronic transition dipole can be locally mapped by the transition density distributions as shown in Figures S8–S11 in the Supporting Information) from being delocalized over the whole (including the central borazine core) molecule for transition iv to being localized on the aryl side groups in iii and only on a couple of phenyl or mesityl rings, respectively, for excitations ii and i. The increasing localization of the electronic transition dipole as a function of the decreasing transition energy is accompanied by reduced absorption cross sections. Thus, on the basis of these calculations, the
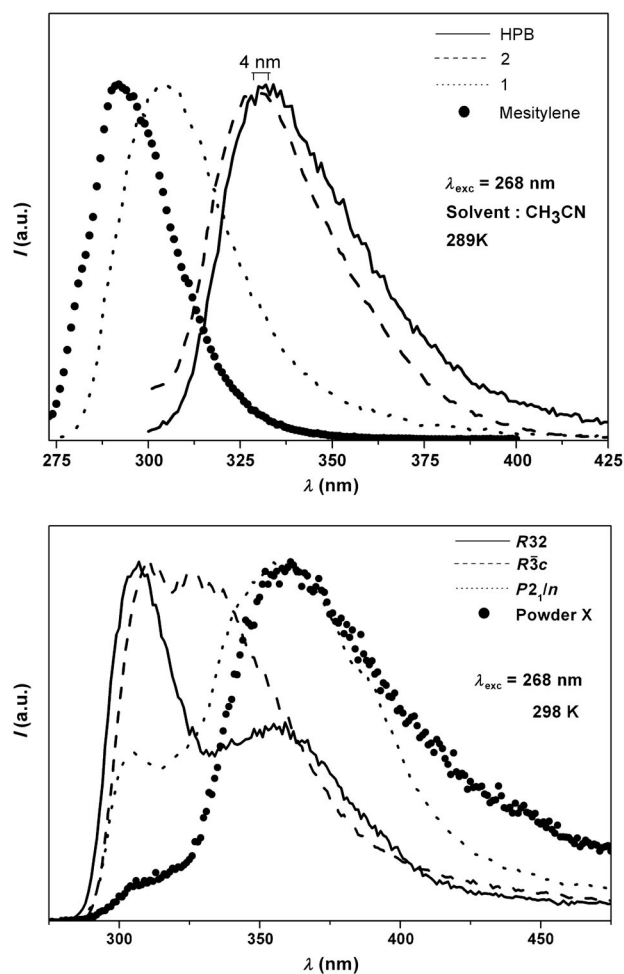
Figure 5. INDO/SCI-simulated absorption spectrum for borazine **1** (dashed trace) together with the corresponding spectrum measured in CH$_3$CN (solid trace). The bands are labeled according to Table 1.

Figure 3. Top: Normalized emission spectra ($\lambda_{exc} = 268$ nm) of borazines **1** and **2** and of reference molecules mesitylene and HPB in CH$_3$CN. Bottom: Normalized emission spectra ($\lambda_{exc} = 264$ nm) of the different borazine polymorphs in the solid state: polymorph space group *R*32 (solid line), *R*$\bar{3}$*c* (dashed line), *P*2$_1$/*n* (dotted line), and ground powder (full circle).

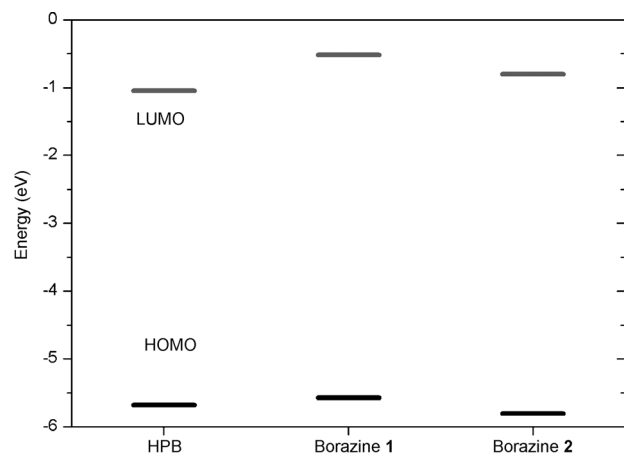Figure 4. DFT/HSE one-electron energy diagram of borazines **1** and **2** in comparison to reference all-carbon HPB analogue.
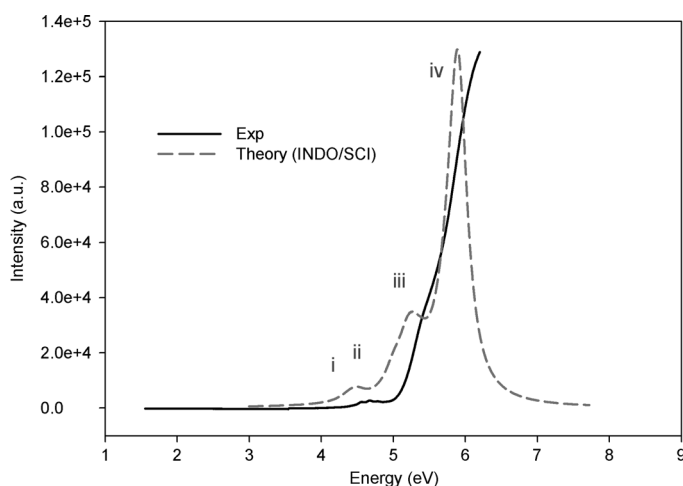
emission bands observed in solution at approximately 310 nm (4 eV) can be assigned to the electronic excited states that belong to the calculated band i. This interpretation is reasonable because the integrated INDO/SCI oscillator strength over that band of 1.3×10^{-2} translates to a radiative (gas-phase) lifetime value of 94 ns, which is in excellent agreement with the value of 92 ns as experimentally estimated from the measured total lifetime and quantum efficiency values in CH$_2$Cl$_2$ (see above). Notably, the low-emission radiative decay rate is also in line with the limited LED quantum efficiency (see below). One can thus speculate that the presence of a dual-emission signal in the solid (i.e., the two emissive features at approximately 310 and approximately 350 nm with polymorph-dependent relative intensities) arises from a removal of the degeneracy of the electronic excitations associated with band i. This effect is likely induced by conformation constraints imposed on the peripheral aryl groups due to a packing effect, which is expected to differently affect the interplanar angle of the phenyl and mesityl units, respectively. These solid-state effects can potentially slow down nonradiative decay pathways that involve conformational degrees of freedom, a phenomenon known as aggregation-induced emission.[25] It is therefore not surprising that, compared to the emission profiles as obtained from solution studies, the most drastic changes in PL spectra are observed for the highest-density *P*2$_1$/*n* polymorph. We note that INDO/SCI calculations performed on clusters of molecule **1** as arranged in the *R*$\bar{3}$*c*, *R*32, and *P*2$_1$/*n* space groups did not show any significant difference in the emission profile (namely, the presence of the low-energy PL emissive band) with respect to that obtained for the single molecule modeled in the vacuum, thus ruling out any effects that are derived from the excitonic delocalization or the formation of *J*-type aggregates (which is not surprising as dipole interactions are vanishingly small for weakly allowed excitations). According to AM1/SCI calculations, the lowest triplet excited states of **1** in the *P*2$_1$/*n* space group

are located at around 2.4 eV (≈ 517 nm) above the singlet ground state, and thus too far in energy to contribute to the photoluminescence signal at approximately 350 nm (although they might be partly responsible for the broad electroluminescence band that extends far into the visible). However, preliminary investigations of the conformational dynamics of borazine **1** in both the gas phase and in the solid state by using molecular dynamics (MD) simulations (Universal force field, 500 ps simulations in the NVT ensemble at 300 K) showed that the conformation of the peripheral aryl groups significantly varies when going from an isolated molecule (in which the rings are able to flip over the 90° barrier at RT) to the crystals (in which the rotation is locked by packing effects). In addition, one can observe that the three mesityl substituents of **1** experience different chemical environments owing to the specific intermolecular interactions in the $P2_1/n$ polymorph, unlike the $R32$ polymorph in which the torsion histograms are essentially superimposable (Figure S26 in the Supporting Information). In principle, this asymmetry is expected to remove the degeneracy associated with the lowest electronic excitations and reshuffle the distribution of the oscillator strengths. INDO/SCI calculations performed on 200 snapshots extracted from the MD simulations indicate an energy splitting of approximately 0.1 eV, which is in line (albeit smaller) with the experimental energy difference of approximately 0.56 eV observed between the two emission peaks for polymorph $P2_1/n$.

Engineering of LED and LEC devices: We also prepared LEDs and LECs that incorporated borazine **1** in the active layer to investigate the emission properties under electrical injection conditions. As with all materials that emit towards the blue/UV end of the available spectrum,[26] charge injection tends to be more difficult than with lower-gap materials as a result of the increased difficulty of matching the work function of the electrodes with the higher-lying lowest-unoccupied molecular orbitals (LUMOs) and the lower-lying highest-occupied molecular orbitals (HOMOs). In particular, the relatively low electron affinity (-1.0 to -1.3 eV) of molecule **1** makes electron injection a challenge compared to hole injection. The best results were expected with an LEC architecture, in which the active material is blended with an ion-transporting polymer such as polyethylene oxide (PEO) and a salt[27] to exploit the buildup of mobile ions at the electrode interfaces to reduce charge-injection barriers. However, we also fabricated and characterized LEDs that incorporated an active layer made of the neat derivative **1** and obtained nearly comparable results. The device structure is shown as an inset in Figure 6 for the LECs and LEDs, and is built on an indium–tin oxide (ITO) anode, with an 80 nm hole-injection layer of poly(3,4-ethylenedioxythiophene) (PEDOT)/polysodium styrene sulfonate (PSS) spin-cast from a 2.8% solution in water (Sigma Aldrich 560596). The active layer consisted either of a blend of emitter **1**, polyethylene oxide as the ion transporter, and lithium triflate (LiOTf) as the salt that provided mobile ions

for the LECs, or of molecule **1** for the LEDs. For LECs, the solution was spin-cast from a mix of toluene and THF (1:1), with a concentration of 2 wt% of solids, of which 50 wt% was borazine **1**, and 50 wt% was PEO/LiOTf with a 20:1 molar ratio of the CH_2CH_2O moieties in PEO to LiOTf. We instead used toluene as a solvent for the LEDs with a 2 wt% concentration of borazine emitter **1**. A low work function anode of LiF (6 nm)/Ca (30 nm)/Al (150 nm) was evaporated to facilitate electron injection, which as mentioned above is notoriously difficult for high-gap materials. The current density and radiance versus voltage characteristics of a typical LEC that incorporates molecule **1** and those of an LED are depicted in Figure 6a,c. Charge injection into the LEC is clearly observed, with a strongly nonlinear dependence of the current density J on the applied voltage V, as is typical for organic and polymeric LEDs. We achieved current densities of >100 mA cm^{-2} at somewhat higher voltages (≈ 15 V) than we would expect for most molecular diodes and LECs. We consider this an indication of the intrinsically low charge mobility in molecule **1**, and of the existence of further margins for optimization of charge transport and possibly of injection. The current turn-on voltage (arbitrarily defined at 10^{-3} mA cm^{-2}) is observed at approximately 3 V, whereas a clearly observable change of slope in the JV characteristics suggests that bipolar injection is achieved at approximately 5 V, which is only marginally higher than the energy gap of the "bluest polymorphs" as inferred from the PL spectra, in line with the results for "organic LECs" in which emission is observed at voltages similar to the modulus of the energy gap (in eV).

Concomitant luminescence was observed with a threshold of approximately 9.5 V (Figure 6a), in which this is defined as the voltage at which the radiance reaches 0.2 mW m^{-2} (owing to the presence of emission in the UV range, at wavelengths <400 nm, we reported the optical output in radiometric units, that is, radiance in mW m^{-2}, rather than photometric units, or luminance in cd m^{-2}), which clearly exceeded our noise level (≈ 0.1 mW m^{-2}). The slight discrepancy in the radiative emission turn-on voltage with respect to the occurrence of bipolar injection is a result of the higher noise in our detection electronics relative to the radiative emission, owing to extrinsic factors (different noise levels in the measurement of the current and radiative emission). Similar results were found for the representative LED, the characteristics of which are reported in Figure 6c, although they show slightly higher noise, and the external quantum efficiency is approximately an order of magnitude higher than that for the LECs. The spectral distribution of the emission, as reported in Figure 6d, clearly demonstrates emission at wavelengths below 400 nm, albeit with a broad spectrum that spans the whole of the visible range as well. Similar results were found for the LEC, the spectrum of which is displayed in Figure 6b. In addition, of potential interest for white-emitting LEDs and applications in the illumination sector, or for backlights, we note that a very large spectral width is in fact to be expected on the basis of the various polymorphs identified, and the possible existence of
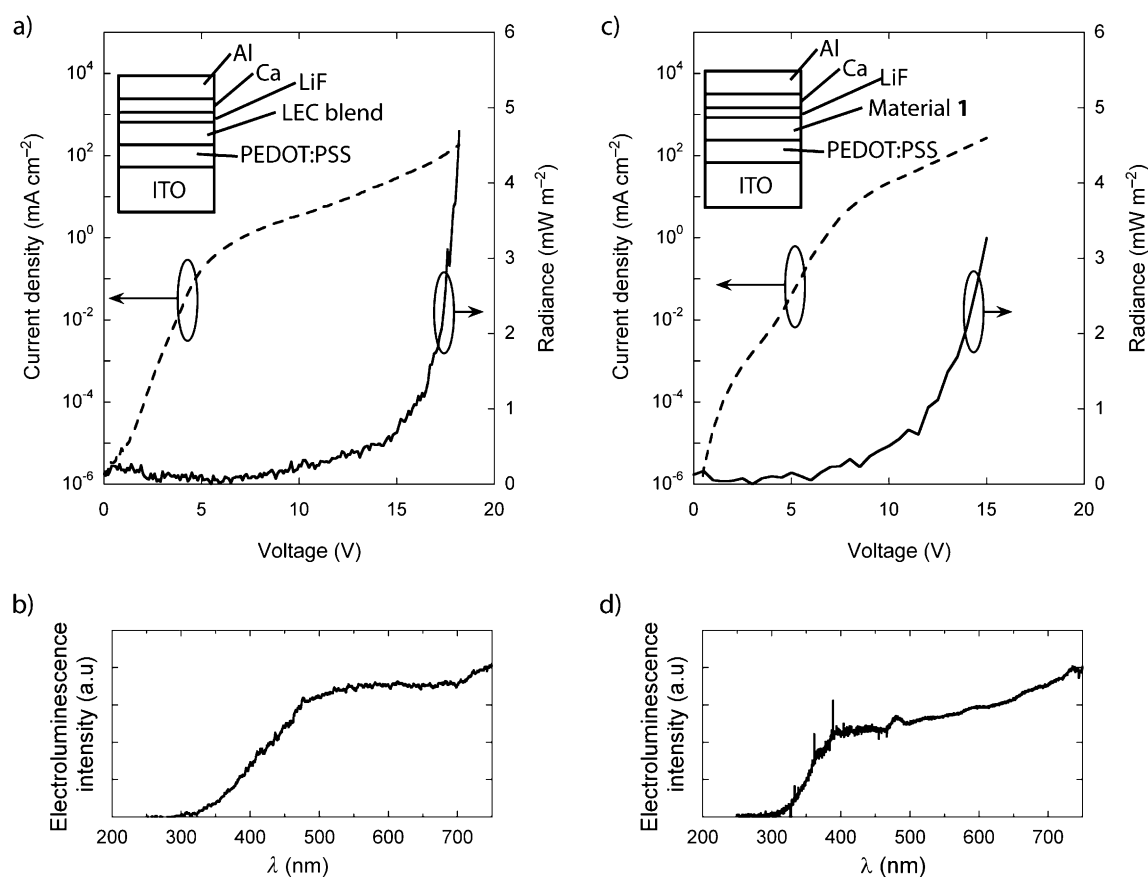
Figure 6. a) Current and radiance versus light characteristics of an LEC incorporating an active layer of emitter **1**, blended with PEO as the ion transporter and LiOTf as the salt that provides mobile ions. The 3.5 mm^2 device was fabricated with the vertical structure ITO/PEDOT:PSS (80 nm)/active layer/LiF (6 nm)/Ca (30 nm)/Al (150 nm), which is indicated schematically as an inset. b) The electroluminescence spectrum obtained at a bias of 17 V of such a device, showing broad emission from the near-UV through the visible spectrum. c) Current/voltage/light characteristics of an LED incorporating an active layer of emitter **1**. The 3.5 mm^2 device was fabricated with the vertical structure ITO/PEDOT:PSS (80 nm)/active layer/LiF (6 nm)/Ca (30 nm)/Al (150 nm). d) The EL spectrum of such a device obtained at a bias of 13.8 V, showing broad emission from the near-UV through the visible spectrum.

other polymorphs not yet identified in our fundamental characterization of the materials. Furthermore, application of electric fields, charge transport, and potential mild heating during device operation might indeed favor the formation of a mixture of polymorphs. A discrepancy between PL and electroluminescent (EL) emission has been observed in the past for some early blue-emitting materials, which was mainly caused by the formation of aggregates, excimers, or exciplexes.[26a] Formation of aggregated species could also be responsible for relatively low EL quantum efficiency[28] as reported here ($\approx 10^{-4}$ %).

Conclusion

In conclusion, we have prepared a new UV-emitting borazine derivative that bears mesityl substituents and displays exceptional chemical stability toward hydrolysis. Detailed crystallographic and fluorescence characterizations showed the existence of several polymorphs, each of which showed a different emission profile in the solid state, thus suggesting a unique interplay between intermolecular forces and the spectroscopic response. In particular, by using molecular dynamics (MD) simulations, computational investigations of the conformational dynamics of borazine **1** in both the gas phase and in the solid state showed that the conformation of the peripheral aryl groups significantly varies when going from an isolated molecule (in which the rings are able to flip over the 90° barrier at RT) to the crystals (in which the rotation is locked by packing effects), thus generating different chemical environments in the different polymorphs owing to the specific intermolecular interactions. This asymmetry is expected to remove the degeneracy associated with the lowest electronic excitations and to reshuffle the distribution of the oscillator strengths, thereby generating an energy splitting that is responsible for the two-peak emissive behavior. In parallel, we have been able to exploit their electroluminescent properties in LEDs and LECs that incorporate borazine **1** as the active material in the emissive layer. Despite a relatively low EL quantum efficiency ($\approx 10^{-4}$ %) and broad emission spectra, this is the first report of UV electroluminescence from borazine-based materials, and we thus consider these data to be particularly encouraging for the prospects of borazine-based devices. The use of

different transparent conducting oxides as anodes or cathodes, or an inverted top-emitting structure with sputtered transparent ITO anodes[29] appears to be entirely plausible, given enough time and critical mass of research devoted to BN-based materials, with potentially disruptive consequences on spectral tunability, efficiency, and device lifetime, as has already happened for organic analogues in the last two decades or so.

Experimental Section

CCDC-897038 ($R32$ for borazine **1**), 897039 ($P2_1/n$ for borazine **1**), 897040 ($R\bar{3}c$ for borazine **1**), and 897046 ($Pna2_1$ for borazine **2**) contain the supplementary crystallographic data for this paper. These data can be obtained free of charge from The Cambridge Crystallographic Data Centre via www.ccdc.cam.ac.uk/data_request/cif.

Acknowledgements

[1] a) L. Chen, Y. Hernandez, X. Feng, K. Müllen, *Angew. Chem. Int. Ed.* **2012**, *51*, 7640–7654; b) J. S. Wu, W. Pisula, K. Müllen, *Chem. Rev.* **2007**, *107*, 718–747; c) F. Diederich, *Chem. Commun.* **2001**, 219–227; d) R. E. Martin, F. Diederich, *Angew. Chem.* **1999**, *111*, 1440–1469; *Angew. Chem. Int. Ed.* **1999**, *38*, 1350–1377; e) D. M. Guldi, B. M. Illescas, C. M. Atienza, M. Wielopolski, N. Martín, *Chem. Soc. Rev.* **2009**, *38*, 1587–1597; f) K. Müllen, J. P. Rabe, *Acc. Chem. Res.* **2008**, *41*, 511–520; g) L. Maggini, D. Bonifazi, *Chem. Soc. Rev.* **2012**, *41*, 211–240; h) V. Palermo, E. Schwartz, C. E. Finlayson, A. Liscio, M. B. J. Otten, S. Trapani, K. Müllen, D. Beljonne, R. H. Friend, R. J. M. Nolte, A. E. Rowan, P. Samorì, *Adv. Mater.* **2010**, *22*, E81–E88; i) S. S. Babu, H. Möhwald, T. Nakanishi, *Chem. Soc. Rev.* **2010**, *39*, 4021–4035; j) S. S. Babu, S. Prasanthkumar, A. Ajayaghosh, *Angew. Chem.* **2012**, *124*, 1800–1810; *Angew. Chem. Int. Ed.* **2012**, *51*, 1766–1776; k) A. Ajayaghosh, *Chem. Soc. Rev.* **2003**, *32*, 181–190.

[2] a) L. Schmidt-Mende, A. Fechtenkötter, K. Müllen, E. Moons, R. H. Friend, J. D. MacKenzie, *Science* **2001**, *293*, 1119–1122; b) A. J. Berresheim, M. Müller, K. Müllen, *Chem. Rev.* **1999**, *99*, 1747–1785; c) K. V. Rao, S. J. George, *Org. Lett.* **2010**, *12*, 2656–2659; d) W. W. H. Wong, D. J. Jones, C. Yan, S. E. Watkins, S. King, S. A. Haque, X. M. Wen, K. P. Ghiggino, A. B. Holmes, *Org. Lett.* **2009**, *11*, 975–978.

[3] a) E. R. Abbey, L. N. Zakharov, S. Y. Liu, *J. Am. Chem. Soc.* **2011**, *133*, 11508–11511; b) A. J. V. Marwitz, A. N. Lamm, L. N. Zakharov, M. Vasiliu, D. A. Dixon, S. Y. Liu, *Chem. Sci.* **2012**, *3*, 825–829; c) M. J. D. Bosdet, C. A. Jaska, W. E. Piers, T. S. Sorensen, M.

Parvez, *Org. Lett.* **2007**, *9*, 1395–1398; d) C. A. Jaska, D. J. H. Emslie, M. J. D. Bosdet, W. E. Piers, T. S. Sorensen, M. Parvez, *J. Am. Chem. Soc.* **2006**, *128*, 10885–10896.

[4] a) E. R. Abbey, L. N. Zakharov, S. Y. Liu, *J. Am. Chem. Soc.* **2008**, *130*, 7250–7252; b) A. Chrostowska, S. Xu, A. N. Lamm, A. Mazie, C. D. Weber, A. Dargelos, P. Baylère, A. Graciaa, S. Y. Liu, *J. Am. Chem. Soc.* **2012**, *134*, 10279–10285; c) P. G. Campbell, E. R. Abbey, D. Neiner, D. J. Grant, D. A. Dixon, S. Y. Liu, *J. Am. Chem. Soc.* **2010**, *132*, 18048–18050; d) A. J. V. Marwitz, M. H. Matus, L. N. Zakharov, D. A. Dixon, S. Y. Liu, *Angew. Chem.* **2009**, *121*, 991–995; *Angew. Chem. Int. Ed.* **2009**, *48*, 973–977; e) Z. Liu, T. B. Marder, *Angew. Chem.* **2008**, *120*, 248–250; *Angew. Chem. Int. Ed.* **2008**, *47*, 242–244.

[5] M. Côté, P. D. Haynes, *J. Phys. Condens. Matter* **2002**, *14*, 9997–10009.

[6] a) A. Stock, E. Pohland, *Ber. Dtsch. Chem. Ges.* **1926**, *59B*, 2215–2223; b) E. K. Mellon, J. J. Lagowski, *Adv. Inorg. Chem. Radiochem.* **1963**, 5, 259–305; c) K. Niedenzu, J. W. Dawson, *Boron-Nitrogen compounds*, Academic Press, New York, **1965**.

[7] S. Kervyn, T. Nakanishi, J. Aimi, A. Saeki, S. Seki, B. Champagne, D. Bonifazi, *Chem. Lett.* **2012**, *41*, 1210–1212.

[8] a) J. P. Doering, A. Gedanken, A. P. Hitchcock, P. Fischer, J. Moore, J. K. Olthoff, J. Tossel, K. Raghavachari, M. B. Robin, *J. Am. Chem. Soc.* **1986**, *108*, 3602–3608; b) R. Islas, T. Heine, G. Merino, *Acc. Chem. Res.* **2012**, *45*, 215–228; c) S. Pelloni, G. Monaco, P. Lazzeretti, R. Zanasi, *Phys. Chem. Chem. Phys.* **2011**, *13*, 20666–20672; d) B. H. Bock, W. Fuss, *Angew. Chem.* **1971**, *83*, 169–170; *Angew. Chem. Int. Ed. Engl.* **1971**, *10*, 182–183.

[9] M. Côté, P. D. Haynes, C. Molteni, *Phys. Rev. B* **2001**, *63*, 125207.

[10] a) C. Gao, M. Pei, Q. Pan, *Asian J. Chem.* **2012**, *24*, 2899–2902; b) X. Fang, L. Hu, K. Huo, B. Gao, L. Zhao, M. Liao, P. K. Chu, G. Bando, D. Golberg, *Adv. Funct. Mater.* **2011**, *21*, 3907–3915; c) S. Xu, C. Xu, Y. Liu, Y. Hu, R. Yang, Q. Yang, J. H. Ryou, H. Jin Kim, Z. Lochner, S. Choi, R. Dupuis, Z. Lin Wang, *Adv. Mater.* **2010**, *22*, 4749–4753; d) S. Park, T. Vogt, *J. Am. Chem. Soc.* **2010**, *132*, 4516–4517; e) Y. Park, J. H. Lee, D. Hyun Jung, S. H. Liu, Y. H. Lin, L. Y. Chen, C. C. Wu, J. Park, *J. Mater. Chem.* **2010**, *20*, 5930–5936; f) K. Geramita, J. McBee, Y. Shen, N. Radu, T. D. Tilley, *Chem. Mater.* **2006**, *18*, 3261–3269; g) T. C. Chao, Y. T. Lin, C. Y. Yang, T. S. Hung, H. C. Chou, C. C. Wu, K. T. Wong, *Adv. Mater.* **2005**, *17*, 992–996.

[11] I. H. T. Sham, C. C. Kwok, C. M. Che, N. Y. Zhu, *Chem. Commun.* **2005**, 3547–3549.

[12] H. C. Brown, V. H. Dodson, *J. Am. Chem. Soc.* **1957**, *79*, 2302–2306.

[13] R. T. Hawkins, W. J. Lennarz, H. R. Snyder, *J. Am. Chem. Soc.* **1960**, *82*, 3053–3059.

[14] K. Nagasawa, *Inorg. Chem.* **1966**, *5*, 442–445.

[15] A. Wakamiya, T. Ide, S. Yamaguchi, *J. Am. Chem. Soc.* **2005**, *127*, 14859–14866.

[16] For a few examples of polymorphism, see: a) A. Gopal, R. Varghese, A. Ajayaghosh, *Chem. Asian J.* **2012**, *7*, 2061–2067; b) G. Zhang, J. Lu, M. Sabat, C. L. Fraser, *J. Am. Chem. Soc.* **2010**, *132*, 2160–2162; c) S. Kohmoto, R. Tsuyuki, H. Masu, I. Azumaya, K. Kishikawa, *Tetrahedron Lett.* **2008**, *49*, 39–43; d) T. Mutai, H. Satou, K. Araki, *Nat. Mater.* **2005**, *4*, 685–687; e) H. Zhang, Z. Zhang, K. Ye, J. Zhang, Y. Wang, *Adv. Mater.* **2006**, *18*, 2369–2372.

[17] a) C. A. Brown, A. W. Laubengayer, *J. Am. Chem. Soc.* **1955**, *77*, 3699–3700; b) S. J. Groszos, S. F. Stafiej, *J. Am. Chem. Soc.* **1958**, *80*, 1357–1360.

[18] a) B. C. Smith, L. Thakur, *Nature* **1965**, *208*, 74–75; b) D. Lux, W. Schwarz, H. Hess, *Cryst. Struct. Commun.* **1979**, *8*, 33–40.

[19] M. J. S. Dewar, E. G. Zoebisch, E. F. Healy, J. J. P. Stewart, *J. Am. Chem. Soc.* **1985**, *107*, 3902–3909.

[20] J. Ridley, M. Zerner, *Theor. Chim. Acta* **1973**, *32*, 111–134.

[21] J. Heyd, G. E. Scuseria, M. Ernzerhof, *J. Chem. Phys.* **2003**, *118*, 8207–8215.

[22] V. A. Rassolov, M. A. Ratner, J. A. Pople, P. C. Redfern, L. A. Curtiss, *J. Comput. Chem.* **2001**, *22*, 976–984.

[23] T. Yanai, D. P. Tew, N. C. Handy, *Chem. Phys. Lett.* **2004**, *393*, 51–57.

[24] Y. Tawada, T. Tsuneda, S. Yanagisawa, T. Yanai, K. Hirao, *J. Chem. Phys.* **2004**, *120*, 8425–8433.

[25] Y. Hong, J. W. Y. Lam, B. Z. Tang, *Chem. Soc. Rev.* **2011**, *40*, 5361–5388.

[26] a) W.-X. Jing, A. Kraft, S. C. Moratti, J. Grüner, F. Cacialli, P. J. Hamer, A. B. Holmes, R. H. Friend, *Synth. Met.* **1994**, *67*, 161–163; b) X.-C. Li, T. M. Yong, J. Grüner, A. B. Holmes, S. C. Moratti, F. Cacialli, R. H. Friend, *Synth. Met.* **1997**, *84*, 437–438; c) Q. Pei, G. Yu, C. Zhang, Y. Yang, A. J. Heeger, *Science* **1995**, *269*, 1086–1088.

[27] a) J. Morgado, F. Cacialli, R. H. Friend, B. S. Chuah, H. Rost, A. B. Holmes, *Macromolecules* **2001**, *34*, 3094–3099; b) J. Morgado, R. H. Friend, F. Cacialli, B. S. Chuah, S. C. Moratti, A. B. Holmes, *J. Appl. Phys.* **1999**, *86*, 6392.

[28] F. Cacialli, J. S. Wilson, J. J. Michels, C. Daniel, C. Silva, R. H. Friend, N. Severin, P. Samorì, J. P. Rabe, M. J. O'Connell, P. N. Taylor, H. L. Anderson, *Nat. Mater.* **2002**, *1*, 160–164.

[29] N. Johansson, F. Cacialli, K. Z. Xing, G. Beamson, D. T. Clark, R. H. Friend, W. R. Salaneck, *Synth. Met.* **1998**, *92*, 207–211.